Research Updates

Advanced single-crystal layered Ni-rich cathode materials for next-generation high-energy-density and long-life Li-ion batteries

Jianming Sun [1,2] Xin Cao [1,2,*] and Haoshen Zhou [1,2,3,†]

[1]*Energy Technology Research Institute, National Institute of Advanced Industrial Science and Technology (AIST), 1-1-1 Umezono, Tsukuba 305-8568, Japan*

[2]*Graduate School of System and Information Engineering, University of Tsukuba, 1-1-1 Tennoudai, Tsukuba 305-8573, Japan*

[3]*Center of Energy Storage Materials & Technology, College of Engineering and Applied Sciences, Jiangsu Key Laboratory of Artificial Functional Materials, National Laboratory of Solid State Microstructures, and Collaborative Innovation Center of Advanced Microstructures, Nanjing University, Nanjing 210093, People's Republic of China*

(Received 31 October 2021; accepted 13 June 2022; published 13 July 2022)

Benefiting from the high specific capacity and output voltage, Ni-rich layered oxides are one of the most promising commercial cathodes for next-generation high-energy-density Li-ion batteries (LIBs). However, typical Ni-rich cathode materials generally inherit polycrystal (PC) morphology from their precursors, which induces severe crack generations and side reactions, resulting in the rapid decay of structural and electrochemical stability upon cycling. In contrast, the Ni-rich cathodes with single-crystal (SC) morphology display remarkable structural stability and long cycle life by means of superior mechanical strength and limited side reactions, which is expected to solve the instinctive problems of PC counterparts. Herein, the synthesis strategies and the growth mechanisms of SC Ni-rich oxides are introduced and summarized in detail. Moreover, the significant differences in electrochemical behaviors between PC and SC cathodes are comprehensively compared in various voltage windows. Furthermore, the corresponding structural evolutions and morphology changes are also systematically investigated and analyzed. Additionally, the state-of-the-art characterization techniques for SC materials are elaborated. Altogether, in this review, we not only unravel the fundamental understandings of SC Ni-rich cathode materials but also provide an effective guide for realizing high-energy-density LIBs with long cycle life.

DOI: 10.1103/PhysRevMaterials.6.070201

I. INTRODUCTION

To meet the increasing demands of energy storage devices, especially for electric vehicles, the development of high-energy-density and long-life cathode materials has been the top priority in the field of Li-ion batteries (LIBs) [1–4]. Layered Ni-rich oxide cathode materials $LiNi_xCo_yMn_zO_2$ ($x \geqslant 0.5$, $x + y + z = 1$) typically display the remarkably high specific capacity and output voltage, which are generally considered the most promising cathode materials for next-generation high-energy-density LIBs [5–7]. More importantly, the energy density of Ni-rich cathode materials can be further improved by increasing Ni content in the chemical formula and broadening the voltage window [8]. However, the traditional layered Ni-rich cathode materials generally possess polycrystal (PC) morphology, which always suffers from severe cracks in the secondary particles [9,10], serious side reactions with electrolytes [11], and volume changes [12] during Li^+ (de)intercalation processes. As a result, especially in high-voltage regions, obvious capacity deterioration and rapid decline of voltage fade can be observed within PC Ni-rich cathode materials [13,14]. Most works mainly focus on modification strategies such as surface coating and doping based on PC morphology [15–17]. Therefore, there is a lack of direct strategies to optimize the structural stability and electrochemical performance of Ni-rich cathode materials which can effectively solve the intrinsic issues of PC counterparts [18,19].

Recently, Li *et al.* [20] developed a big family of single-crystal (SC) Ni-rich cathode materials, which realized ultralong cycling life in pouch full cells by coupling with artificial graphite as the anode material. SC $LiNi_{0.5}Mn_{0.3}Co_{0.5}O_2$ delivered the remarkable capacity retentions of ~92% after 4700 cycles between 3 and 4.3 V [21]. Based on the excellent electrochemical stability upon long-term cycling, the Tesla company proposed the million-mile battery plan by employment of Ni-rich cathode materials with SC morphology. When increasing the Ni-content, SC $LiNi_{0.8}Mn_{0.1}Co_{0.1}O_2$ also reached excellent capacity retention of ~98% after 1200 cycles and 94% after 2250 cycles between 3 and 4.2 V, respectively, whereas the PC counterpart suffered from obvious capacity decay and delivered lower capacity retention of 91% after 200 cycles at the same electrochemical conditions [22,23]. The significant performance differences can be attributed by the serious crack generation within the PC sample and the severe side reactions on the cathode-electrolyte interface upon long cycling [24]. Benefiting from the unique features such as crack-free morphology and low specific surface, the design of SC morphology can be regarded as an effective strategy for Ni-rich cathodes to harvest the

*cao.xin@aist.go.jp
†hszhou@nju.edu.cn

excellent structural stability and superior cycle performance during long-term cycling. Additionally, there are some issues slowing the development and application of SC Ni-rich cathode materials. For instance, the growth control of uniform large-sized particles is an obvious challenge in the synthesis section of SC Ni-rich materials, which has a significant influence on electrochemical performances such as output capacity and cycling stability. The grain growth processes in various preparation methods and conditions have not been clearly summarized. Furthermore, the mechanisms of structural deterioration and induced capacity decay, especially in high-voltage ranges, still need to be further clarified, which is beneficial for unraveling the underlying reasons for high-voltage stability in SC Ni-rich electrodes. In addition, state-of-the-art techniques for characterizing the structural evolutions and morphology changes upon cycling in SC cathode materials should be comprehensively introduced [25–28].

Herein, the preparation strategies of SC Ni-rich layered cathode materials are summarized in detail, in which the high-temperature, multicalcination, spray pyrolysis and molten salt assistant methods, and corresponding characteristics are introduced. Moreover, the differences in electrochemical activities and structural stability between SC and PC electrodes are comprehensively compared in both low- and high-voltage windows. Furthermore, the morphology changes and structural evolutions such as layered spinel–rock-salt phase transitions are clearly presented, in which the underlying mechanisms of structural and electrochemical failure are proposed within both SC and PC layered Ni-rich cathodes, respectively. In addition, a series of techniques including cross-sectional scanning electron microscope (SEM) imaging and three-dimensional (3D) reconstruction for characterizing SC Ni-rich materials is introduced, which is beneficial for providing solid and effective evidence to unravel the failure mechanisms of SC Ni-rich and other cathode materials. In this review, we provide fundamental understandings of SC Ni-rich cathode materials, especially from the material physics perspective, and propose an effective guideline for further realizing next-generation high-energy-density LIBs with long cycle life.

II. SYNTHESIS METHODS OF SC LAYERED NI-RICH CATHODE MATERIALS

The morphology, structure, and electrochemical performances of both PC and SC Ni-rich cathode materials generally depend on the preparation methods and conditions [29]. The traditional synthesis strategy of PC Ni-rich materials generally adopts the composite method of coprecipitation and high-temperature calcination [30]. The precursors of transition metal hydroxides or oxides with uniform morphology were employed to prepare PC Ni-rich materials after calcination with Li salts at high temperature [31]. The preparation of SC Ni-rich materials also needs the uniform precursor, and the subsequent synthesis processes have significant effects on grain sizes, shapes, and crystal orientations [32], in which high-temperature calcination [33], multicalcination [34], the molten salt method [35], and spray pyrolysis [36] were widely conducted. Trevisanello *et al.* [33] developed the SC $LiNi_{0.8}Co_{0.1}Mn_{0.1}O_2$ cathode material with size particles of 1–3 μm via the traditional high-temperature calcination method [Fig. 1(a)]. The $Ni_{0.8}Co_{0.1}Mn_{0.1}(OH)_2$ hydroxide precursor was mixed with excess Li_2CO_3, and the mixture was calcinated at 875 °C for 6 h under an oxygen atmosphere. The SC sample was collected after being washed with deionized water to remove the excess Li_2CO_3 and then calcinated at 600 °C for 3 h in oxygen. Notably, an oxygen atmosphere is necessary to obtain the SC Ni-rich materials, which is beneficial for restraining Li/Ni cation mixing and decreasing the Ni oxidation state [37,38]. Moreover, a high-calcination temperature can accelerate the speed of grain growth, which promotes the formation of SC morphology [39]. This method possesses many advantages such as simple operations and low cost, whereas serious problems existing in SC products prepared by this method since long-time and high-temperature calcination induce cation mixing and impurities of residual lithium, and uniform SC grains in crystallography are difficult to obtain [35,39–41]. Additionally, the particle agglomeration of SC cathode materials is typically prone to appear by high-temperature calcination [41,42].

To address the mentioned issues, the multicalcination strategy was also widely employed. Guo *et al.* [34] prepared SC $LiNi_{0.83}Co_{0.12}Mn_{0.05}O_2$ with uniform particles through the multicalcination process. SC $LiNi_{0.83}Co_{0.12}Mn_{0.05}O_2$ was obtained by calcining the mixture of Li_2CO_3 and $Ni_{0.83}Co_{0.12}Mn_{0.05}(OH)_2$ precursor at 500 °C for 1 h, which was then calcinated at 750 °C for 5 h and finally calcinated at 860 °C for 12 h. The SEM and the transmission electron microscope (TEM) images of the SC sample are shown in Fig. 1(b). The SC sample prepared by this method displayed excellent structural stability and cycle performance, in which the capacity retention reached 88.72% in the pouch cell after 500 cycles at the current density of 63 mA/g. Although this method solved problems such as lithium salt impurities in high-temperature calcination to some extent, the obtained SC particles typically displayed the appearance of agglomeration and nonuniformity. Additionally, the multicalcination method with high temperature was generally considered to tend to form SC morphology, while the preparation of high-nickel contents requires a relatively low calcination temperature, which makes it difficult to harvest Ni-rich cathode materials with SC morphology. Therefore, the synthesis temperature of SC Ni-rich layered cathode materials needs to be further selected and controlled [43–46].

Recently, synthesis methods were introduced in the preparation of SC Ni-rich layered materials. Leng *et al.* [36] prepared the porous oxide precursor of chemically active $LiNi_{0.8}Co_{0.15}Al_{0.05}O_2$ by the spray pyrolysis method, which effectively reduces the calcination temperature and promotes the generation of particles with uniform size. The $Ni_{0.8}Co_{0.15}Al_{0.05}O_x$ precursor was prepared by the transition metals chloride solution being atomized into micron drops by an ultrasonic atomization generator and passed into a three-zone vertical furnace with oxygen flow at 800 °C. The monodisperse and uniform SC $LiNi_{0.8}Co_{0.15}Al_{0.05}O_2$ was obtained by calcining the mixture of the oxide precursor and Li_2CO_3 at 750 °C for 0–20 h in oxygen. To investigate the evolutions from precursor to product during the synthesis process, *ex situ* SEM was performed to track the morphology changes from 0 to 20 h at 750 °C. At the initial state, Li_2CO_3 and the

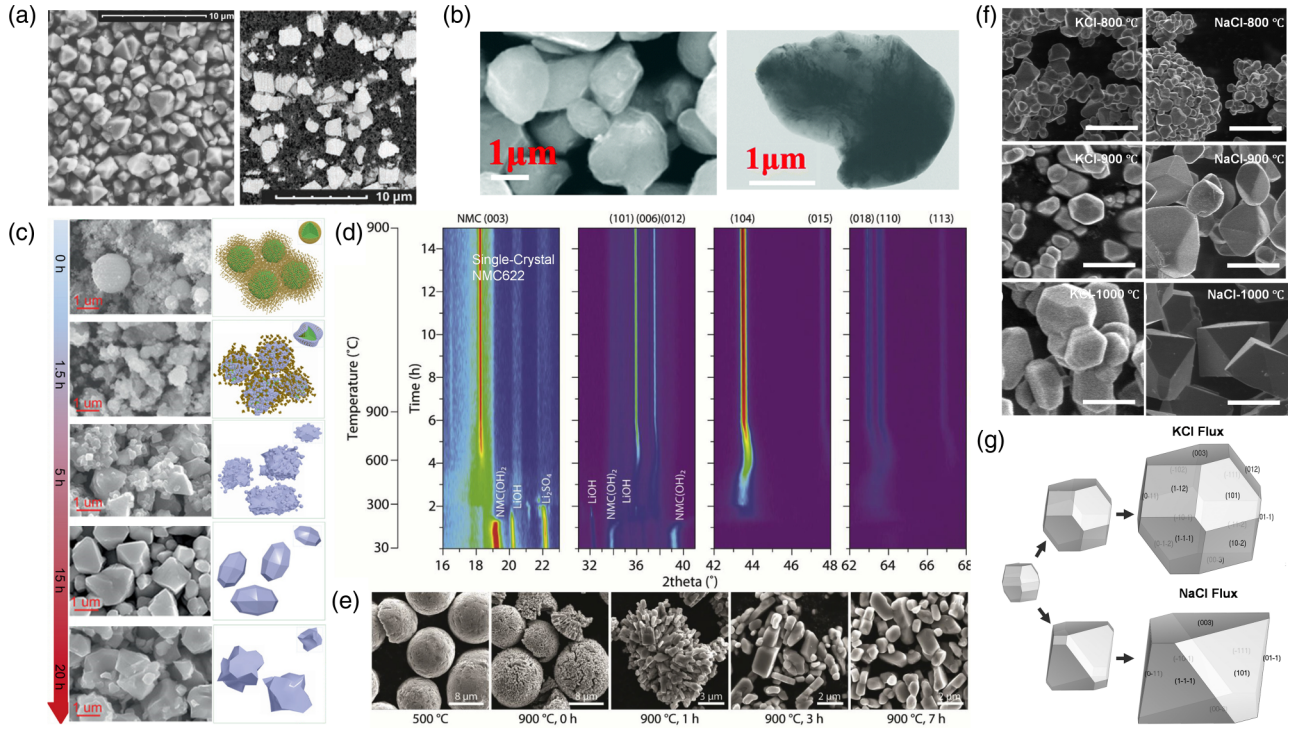

FIG. 1. (a) Scanning electron microscope (SEM) and cross-sectional SEM images of the single-crystal (SC) $LiNi_{0.8}Co_{0.1}Mn_{0.1}O_2$ sample prepared by the high-temperature calcination method. Reproduced with permission [33]. (b) SEM and transmission electron microscope (TEM) images of SC $LiNi_{0.83}Co_{0.12}Mn_{0.05}O_2$ prepared by the multicalcination method. Reproduced with permission [34]. (c) *Ex situ* SEM images and illustrations of the morphology evolution during calcination from 0 to 20 h with the spray pyrolysis precursor of the $LiNi_{0.8}Co_{0.15}Al_{0.05}O_2$ cathode material. Reproduced with permission [36]. (d) Time-resolved *in situ* x-ray diffraction (XRD) patterns during synthesis of the SC $LiNi_{0.6}Mn_{0.2}Co_{0.2}O_2$ material by the molten salt method and (e) corresponding *ex situ* SEM at different temperature and calcination time. Reproduced with permission [48]. (f) Molten-salt synthesis of SC $LiNi_{0.8}Mn_{0.1}Co_{0.1}O_2$. KCl and NaCl salt as flux at 800, 900, and 1000 °C, and (g) responding schematics. Reproduced with permission [35].

spherical precursor can be easily distinguished. With increasing the calcination time, the SC particles gradually formed. After calcination for 15 h, the sample showed monodisperse particles with regular shapes [Fig. 1(c)]. Although this method solved the problem of particle size and agglomeration at high temperatures, it is difficult to apply in the industry at a large scale because of the complicated operation.

The molten salt method was developed to prepare SC layered Ni-rich materials, which is currently the most concerned preparation method to obtain high-quality SC morphology [34]. An excess amount of molten salt was added into the mixture of the precursor and lithium source, in which the molten salt as the flux is melted at high temperature, which significantly boosted the ion diffusion, thereby forming uniform SC particles with large sizes. Moreover, benefiting from the excellent flowability of molten salt, the particles are hard to agglomerate at high temperature. Finally, the sample needs to be washed with deionized water to remove the excess flux salt [47–49]. Qian *et al.* [48] synthesized the SC $LiNi_{0.6}Mn_{0.2}Co_{0.2}O_2$ cathode material with 2-μm-sized particles via scalable molten salt synthesis. The forming process of SC particles at high temperature was clearly detected by time-resolved *in situ* x-ray powder diffraction at various temperatures [Fig. 1(d)]. The mixture of the precursor $Ni_{0.6}Mn_{0.2}Co_{0.2}(OH)_2$, LiOH, and Li_2SO_4 as the flux was calcination at 900 °C. The peaks of the precursor suddenly disappeared at 200 °C because of the decomposition of hydroxides. The peaks of (003) were observed from 600 °C, and the intensity continuously increased with increasing reaction time, which indicates the layered structure was gradually formed with the increase of temperature and holding time. *Ex situ* SEM was also performed to observe the grain growth evolutions of SC samples, which were collected at different calcination times [Fig. 1(e)]. After the temperature reached 900 °C, the spherical oxide precursor grains gradually disintegrated at first, and then the original grains grew to SC morphology with regular crystal facets. This phenomenon can be explained as the particles followed the dissolution-recrystallization mechanism in the molten salt method, which was different from the high-temperature calcination strategy [50,51]. Although uniform SC particles with large size can be prepared by the molten salt method, the influence of significant factors, such as the flux salt and calcination temperature on grain growth, still needs to be further clarified. The different fluxes of the molten salt method have a significant impact on the morphology and structure of the as-prepared SC sample. Kim [35] compared the difference between NaCl and KCl as the flux during the preparation of SC $LiNi_{0.8}Co_{0.1}Mn_{0.1}O_2$. The employment of KCl promoted the generation of sphere particles with different crystal facets, whereas the particles calcined with NaCl displayed the morphology of perfect octahedra shapes. This is mainly attributed to the difference

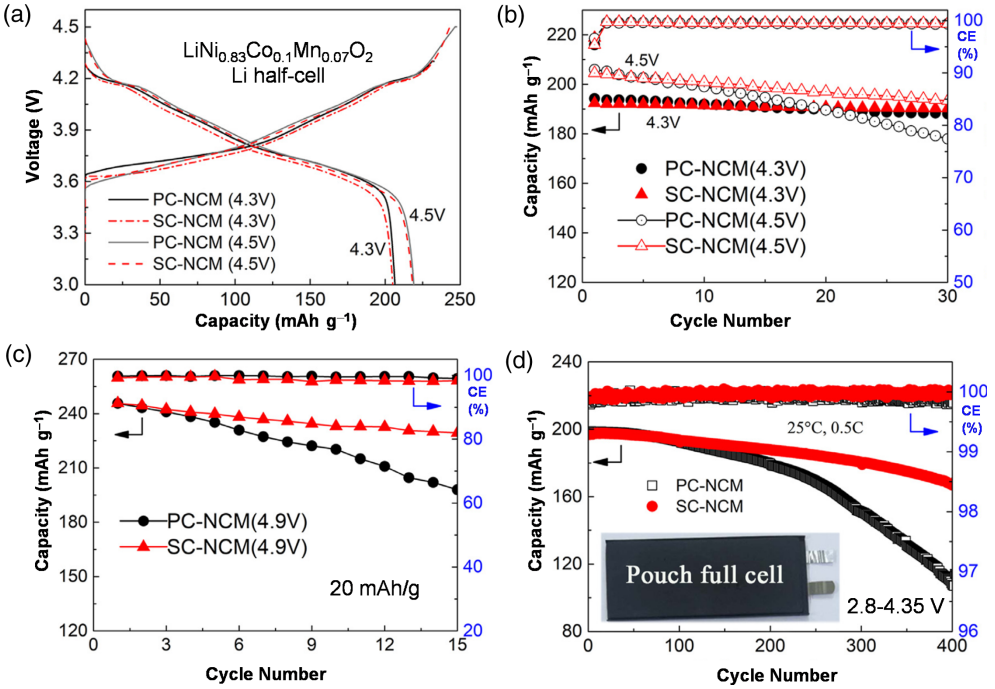

FIG. 2. (a) First charge-discharge profiles of the single-crystal (SC) and polycrystal (PC) Ni-rich $LiNi_{0.83}Co_{0.10}Mn_{0.07}O_2$ cathode material at current density of 20 mA/g, and (b) cycle performance for the cutoff voltages of 4.3 and 4.5 V at current density of 100 mA/g. (c) Cycle performances for the voltage window between 3.0 and 4.9 V at current density of 20 mA/g. (d) Cycle performance in the pouch cells between 3.00 and 4.35 V at current density of 100 mA/g. Reproduced with permission [54].

between the fluxes of KCl and NaCl, especially the properties at liquid phase [Figs. 1(f) and 1(g)]. Crystal orientation was considered closely related to the different energies of interfaces between crystal and molten salt, especially the flux. The flux of KCl led to a decrease of the surface energy difference of the facet, boosting the formation of spherical morphology, while the growth of octahedra shape facets was promoted by the flux of NaCl, in which the morphology changes would further influence the structural stability and electrochemical performance of SC cathode materials.

III. ELECTROCHEMICAL PERFORMANCES OF SC LAYERED NI-RICH CATHODE MATERIALS

PC Ni-rich cathode materials generally suffered from serious capacity decay upon long-term cycling especially in the high-voltage range, which can be mainly attributed to severe layered structure fade, side reactions, and crack generation [52]. Recently, authors of many studies proposed that Ni-rich materials with SC morphology could retain the layered structure and limited volume change, which have the great potential to solve the problems in PC Ni-rich cathode materials, especially at high cutoff voltage, and to harvest superior long-term cycling stability [53–55]. Pang *et al.* [54] developed crack-free SC $LiNi_{0.83}Co_{0.10}Mn_{0.07}O_2$ cathode materials by the high-temperature calcination method which displayed superior cycle performances in both low- and high-voltage ranges (Fig. 2). It was generally considered that the excellent mechanical strength of SC materials can retain the morphology of particles without crack generation upon the Li^+ (de)intercalation processes. According to the initial charge-discharge profiles, both SC and PC $LiNi_{0.83}Co_{0.10}Mn_{0.07}O_2$ electrodes displayed a similar capacity (~210 mAh/g in the voltage range of 3.0–4.3 V and ~220 mAh/g in the voltage range of 3.0–4.5 V), which suggests more output capacity can be utilized at high cutoff voltage of 4.5 V [Fig. 2(a)]. Although PC and SC electrodes exhibited excellent capacity retention in the voltage range from 3.0 to 4.3 V, superior capacity retention of 94.5% can be achieved in SC Ni-rich cathodes after 30 cycles, while PC cathodes possessed poor capacity retention of 86.4% at the same high cutoff voltage [Fig. 2(b)]. The remarkable difference in cycle performance between SC and PC samples was observed at the high cutoff voltage of 4.9 V. Benefiting from the crack-free characteristic, the capacity retention rate of the SC sample reached 93.3% after 15 cycles in the voltage window of 3.0–4.9 V, while the PC sample displayed poor electrochemical stability with the capacity retention of 80.6% [Fig. 2(c)]. In addition, the SC Ni-rich $LiNi_{0.83}Co_{0.10}Mn_{0.07}O_2$ electrode exhibited excellent long-term cycle performance in a pouch full cell with a graphite anode, which displayed excellent capacity retention of 84.8% in comparison with 54.1% of the PC $LiNi_{0.83}Co_{0.10}Mn_{0.07}O_2$ electrode as a cathode in the voltage window of 3.0–4.35 V after 400 cycles at the current density of 100 mA/g [Fig. 2(d)].

Klein *et al.* [55] compared the differences in electrochemical behaviors between SC and PC $LiNi_{0.5}Co_{0.3}Mn_{0.2}O_2$ cathode materials at various cutoff voltages, in which both cathodes were tested in full cells with a graphite anode (Fig. 3). Compared with the initial charge-discharge curves at various cutoff voltages of 4.3, 4.4, and 4.5 V, both PC and SC electrodes displayed similar capacities, in which no obvious voltage decay and irreversible capacity can be observed with widening the voltage ranges [Figs. 3(a) and 3(b)]. Intriguingly, the SC electrode displayed a higher irreversible capacity

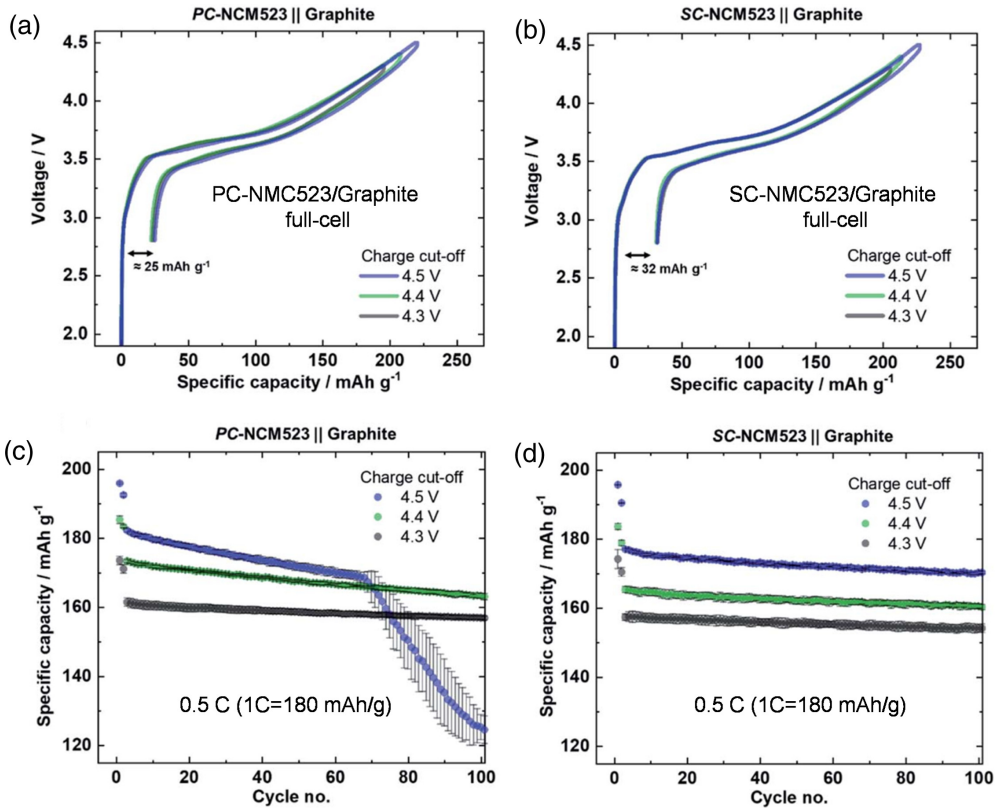

FIG. 3. First two charge-discharge profiles of (a) the polycrystal (PC) and (b) the single-crystal (SC) $LiNi_{0.5}Mn_{0.3}Co_{0.5}O_2$ cathode in full cell with graphite anode at current density of 20 mA/g at cutoff voltages of 4.3, 4.4, and 4.5 V. Cycle performances of (a) the PC and (b) the SC $LiNi_{0.5}Mn_{0.3}Co_{0.5}O_2$ cathode in the full cell at current density of 90 mA/g at cutoff voltages of 4.3, 4.4, and 4.5 V. Reproduced with permission [55].

(32 mAh/g) than 25 mAh/g within the PC electrode at different cutoff voltages during the initial charge and discharge process [Figs. 3(a) and 3(b)], which can be attributed to the sluggish kinetic processes during Li^+ diffusion caused by large SC particles [56]. Moreover, the cycle performances of SC and PC samples tested in different voltage windows are shown in Figs. 3(c) and 3(d). The PC electrodes delivered higher output capacities of ∼160, 172, and 180 mAh/g at cutoff voltages of 4.3, 4.4, and 4.5 V, respectively, in contrast with ∼158, 165, and 175 mAh/g in SC electrodes at the same electrochemical conditions. Significantly, compared with PC electrodes, the Ni-rich SC $LiNi_{0.5}Co_{0.3}Mn_{0.2}O_2$ cathode displayed remarkably excellent cycle performance at cutoff voltages of 4.3, 4.4, and 4.5 V, which indicates the stable layered structure can be well preserved within SC samples. Additionally, the output capacity of the PC sample displayed sudden capacity decay after 70 cycles at the high-voltage window of 4.5 V, while the stable capacity of $>170\,mAh/g$ was still well retained in the SC cathode, which was contributed to the rollover failure triggered by the reduction reactions of transition metals on the anode surface. Therefore, SC Ni-rich layered oxides can be regarded as some of the most promising cathode materials with high-voltage stability upon long-term cycles in comparison with PC counterparts [57].

Additionally, the electrochemical safety is an important factor affecting the application of Ni-rich cathode materials. Suffering from high-energy density and cutoff voltage, the Ni-rich cathode displayed drastic thermal stability fade. Furthermore, the SC Ni-rich electrode at the high-voltage charging state exhibited more stable impedance, thickness, and capacity change than those of the PC, which clarified that the thermal stability improvements of SC nickel, cobalt, manganese (NCM) are ascribed to the depressed side reactions between the cathode and electrolyte [54]. It is generally recognized that gas evolution is known as the main reason for deteriorated safety of Ni-rich cathodes. Differential scanning calorimetry (DSC) is usually performed to evaluate the thermal stability and gas evolution of Ni-rich cathode materials. Guo and Li [58] compared the decomposition temperatures between SC and PC $LiNi_{0.7}Co_{0.15}Mn_{0.15}O_2$ samples (4.5 V charged state) by DSC measurement. The main exothermic peak of the SC sample occurred at 245.5 °C, which was higher than 237.7 °C of the PC sample. Therefore, the structure of SC-NCM can effectively suppress gas release, improving the thermal safety.

IV. STRUCTURE EVOLUTION

To investigate the underlying reasons for electrochemical differences between SC and PC cathode materials, morphology and structural characterizations were performed to detect the crack generation and phase transition upon cycling (Fig. 4). Pang *et al.* [54] systematically tracked the interior morphology changes within SC and PC $LiNi_{0.83}Co_{0.10}Mn_{0.07}O_2$ electrodes at the pristine state and after 200 and 400 cycles [Fig. 4(a) and 4(b)]. Intergranular crack

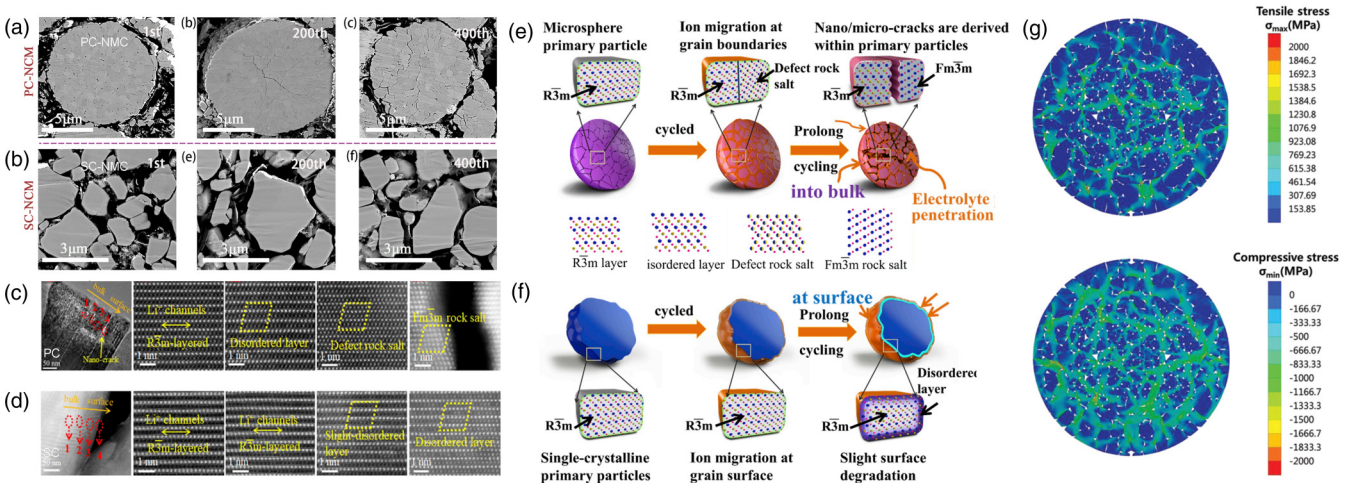

FIG. 4. Cross-sectional scanning electron microscope (SEM) images of (a) polycrystal (PC) and (b) single-crystal (SC) $LiNi_{0.83}Co_{0.10}Mn_{0.07}O_2$ charged to the cutoff 4.35 V for the pristine state and after 200th and 400th cycles. Reproduced with permission [54]. Transmission electron microscope (TEM) and corresponding high-angle annular dark-field scanning transmission electron microscopy (HAADF-STEM) images of (c) PC and (d) SC $LiNi_{0.83}Co_{0.10}Mn_{0.07}O_2$ electrodes at a different location to the crack. Illustration of the relationship between structural evolution and performance fade for (e) PC and (f) SC particles during long-term cycling. Reproduced with permission [61]. (g) Tensile stress and compressive stress distribution for $LiNi_{0.9}Co_{0.05}Mn_{0.05}O_2$ particles at the fully charged state [65].

propagation and structural collapsing can be clearly observed in the PC samples with the increase of cycle numbers, which is generally considered to be caused by the uneven stress and lattice distortion on the surface and inside of the grain [54]. As a result, the crack would greatly increase the specific area of the surface and inevitably accelerate the side reactions between the electrode and electrolyte upon cycling since the Ni-enriched surface of PC particles would catalyze the electrolyte decomposition. These reasons are generally considered failure mechanisms of electrochemical performance in PC Ni-rich cathode materials. In contrast, the pristine morphology of the SC cathode was identical with the sample even after 400 cycles, in which crack generation cannot be detected upon cycling, which effectively boosts the cycle performance of SC Ni-rich cathode materials during long-term cycling [59,60].

The formation and propagation of cracks have significant effects on structural evolutions and electrochemical performance of the Ni-rich cathode material [54]. Scanning transmission electron microscopy (STEM) was performed to clarify structural distortions such as phase transition in PC and SC layered cathode materials upon cycling [Figs. 4(c) and 4(d)]. Figure 4(c) showed the microstructure information of the cycled PC electrode in four local regions near the crack. The layered structure with the space group of $R\bar{3}m$ can be maintained in the region far away from the crack, while the phase transition occurred when approaching the crack region, delivering structural changes from layered to disordered even to defect rock salt. Notably, the harmful rock-salt phase of the $Fm\bar{3}m$ space group can be detected on the surface of the crack. The obvious structural evolution from layered to rock salt suggested PC Ni-rich cathode materials suffered from the serious lattice distortion upon Li^+ (de)intercalation processes. On the contrary, there was no crack generation observed in SC electrodes, in which the layered structure can be well preserved in the bulk material with a slight disordered phase on the surface Fig. 4(d) [61]. The excellent structural stability achieved in SC Ni-rich cathodes can be attributed to the unique features such as being crack free and limited side reactions. The illustration of the proposed interior morphology changes and structural evolution is shown in Figs. 4(e) and 4(f), which clarifies the underlying mechanisms of the electrochemical performance decay and structure fade in PC and SC cathodes during the long-term cycles [61]. For the PC layered Ni-rich cathode, ion migration occurred at grain boundaries, which induced the phase transition from layered to defect rock salt after several cycles. During long-term cycles, obvious cracks generated in the bulk and surface of the PC particles, in which the electrolyte gradually penetrated the secondary particles along the cracks, which caused serious side reactions and induced gas generation and electrolyte decomposition. Additionally, the irreversible metal ion migration accelerates the formation of the rock-salt phase with the space group of $Fm\bar{3}m$ in the bulk and surface, further resulting in serious structural fade and irreversible capacity decay [62]. The reason for crack generation in the intergranular secondary particles was generally regarded as the grain collapsing caused by the anisotropic stress and serious structural distortion in PC layered Ni-rich cathode materials during long-term cycling. [63,64]. In contrast, SC Ni-rich cathode materials showed a different morphology change and structural evolution in comparison with the PC counterpart. Benefiting from excellent mechanical strength, the crack was difficult to generate in the SC particles, further restraining the serious side reaction on the interface between the cathode material and electrolyte. Even after long-term cycles, the excellent layered structure without any phase transition can be realized in bulk material of the SC Ni-rich cathode, in which a slight disordered layer can only be observed on the surface. Significant evidence has demonstrated SC Ni-rich layered cathode materials possess excellent structural and electrochemical stability during long-term cycling.

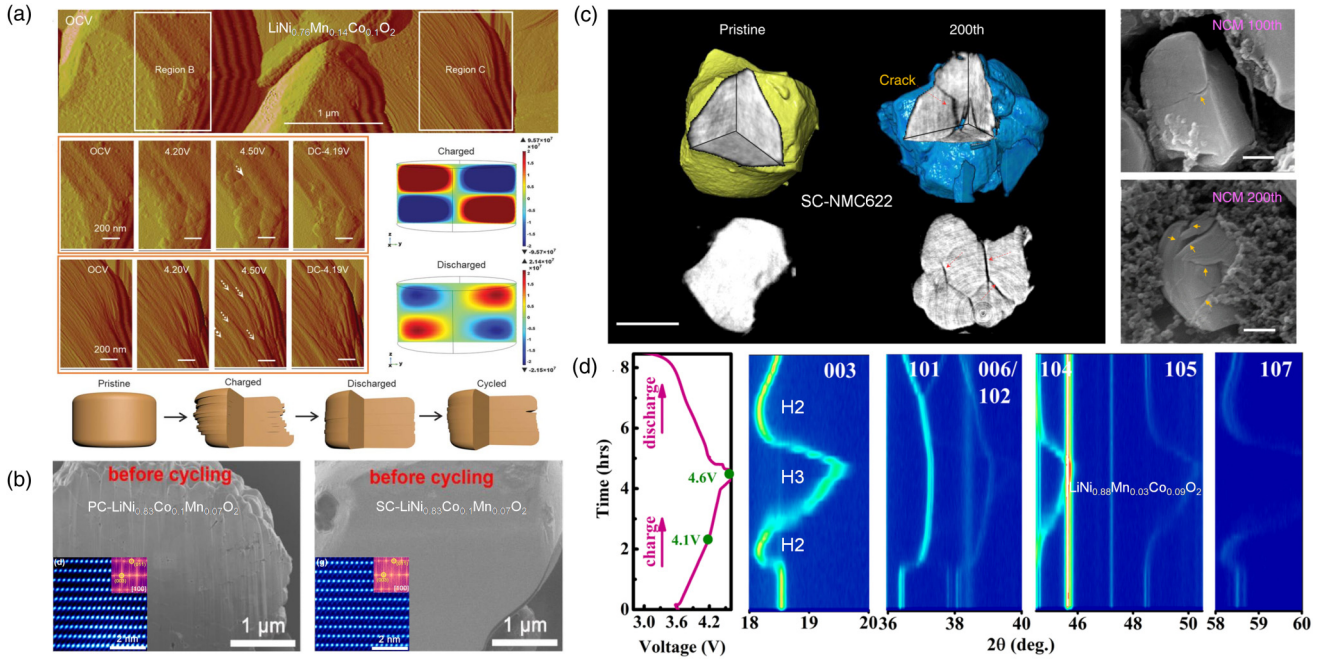

FIG. 5. (a) *In situ* atomic force microscopy (AFM) images of the single-crystal (SC) $LiNi_{0.76}Mn_{0.14}Co_{0.1}O_2$ cathode material during the charge-discharge process, and corresponding calculation results and model. Reproduced with permission [67]. (b) Cross-sectional scanning electron microscope (SEM) images of pristine polycrystal (PC) and SC $LiNi_{0.83}Co_{0.10}Mn_{0.07}O_2$. Insert images are scanning transmission electron microscopy (STEM) images and fast Fourier transform (FFT) results. Reproduced with permission [63]. (c) X-ray nanotomography three-dimensional (3D) reconstruction of SC after cycles and corresponding SEM images. Reproduced with permission [69]. (d) *In situ* x-ray diffraction (XRD) pattern of SC $LiNi_{0.88}Co_{0.09}Mn_{0.03}O_2$. Reproduced with permission [70].

Moreover, intergranular crack generation is also an important physical behavior of Ni-rich materials, which is mainly determined by accumulation and distribution of stress during long-term cycling [65]. Serious volume change occurred in PC Ni-rich materials upon Li^+ (de)intercalation processes, especially at high cutoff voltage, which causes severe stress concentrations and intergranular fracture at the internal grain boundaries in mechanics. A deeply physical analysis of crack generation and growth is beneficial to clarify the electrochemical fade mechanism of Ni-rich materials. To clarify the defect of mechanical stability in PC Ni-rich materials, two-dimensional (2D) finite element analysis is applied to PC Ni-rich cathode materials at charged state.

In addition, the effect of the high-voltage region on the Ni-rich cathode is not only the fade of morphology and structure but also various multiple-failure mechanisms upon the repeated charge-discharge processes, such as gas release, side reaction with the electrode, and dissolution of transition metal elements, which are even further accelerated in the high-voltage regions. In the high-voltage region, the electrolyte decomposition and side reactions lead to gas release, including O_2 and CO_2. Although the gas evolution can be observed in both PC and SC Ni-rich materials, the SC exhibited obviously less gas release benefited from the SC morphology with less specific surface area [66]. A similar advantage of the SC is reflected in the dissolution of transition metal elements. It is generally assumed that the electrolyte is prone to infiltrate the secondary particles with the large specific surface area and intergranular grain boundaries of the PC. The infiltration with the electrolyte will inevitably lead to more drastic dissolution of transfer metal (TM) ions, which are reduced to TM particles on the anode and destroy the electrochemical performance of both the cathode and anode, whereas the failure was suppressed in the SC Ni-rich cathode. Klein *et al.* [55] compared the surface of cycled graphite anodes from the Ni-rich/graphite full cell after 100 cycles for the cutoff voltages of 4.5 and 4.7 V between PC and SC by energy-dispersive x-ray spectroscopy measurement. The graphite anode from the PC cell exhibited obviously higher intensities of TM than those of the SC, which directly suggested more transition metal dissolution than the SC.

V. CHARACTERIZATION TECHNIQUES

To probe the morphology changes and structure evolutions upon (de)lithiation processes, *in situ* and *ex situ* characterizations including atomic force microscopy (AFM), selected area electron diffraction, SEM, STEM, x-ray diffraction (XRD), and 3D reconstruction were performed. Bi *et al.* [67] tracked the surface morphology of SC $LiNi_{0.76}Mn_{0.14}Co_{0.1}O_2$ in the initial charge-discharge process by *in situ* AFM, in which the evolutions of gliding steps and cracks were clearly observed [Fig. 5(a)]. The crack in the SC particle generated during the charge process can be coalesced to the original position upon the discharge process, which effectively clarifies the underlying reason for SC Ni-rich cathode materials being crack free. Significantly, the size and position of this gliding crack were related to the potential change, in which the obvious crack generated at higher voltage ranges. Moreover, the theory calculation provided the results of stress and strain distribution during the charge and discharge processes by employment of COMSOL software. It was found that the shear stress

component was able to promote the gliding on the surface, in which COMSOL can provide the evolution of shear stress component during the charge and discharge processes. Therefore, SC Ni-rich cathode materials can realize the reversibility of gliding upon Li^+ (de)intercalation processes in theory. However, after the discharging process, trace amounts of nanocracks can generate on the surface because of the irreversible (de)lithiation processes. To clarify the more concrete process of surface gliding during charge and discharge processes, the model was built to describe the structure evolution and mechanical behaviors in the SC sample. The cracks were gradually produced after repeated irreversible gliding processes during the long-term cycling, which has slight influence on the electrochemical performances of SC Ni-rich cathode materials.

Cross-sectional SEM is also widely employed to investigate the evolution of internal structure and cracks of SC and PC samples, which is an effective measurement to explain the differences in morphology change between SC and PC electrodes upon cycling [Fig. 5(b)]. Focused ion beam SEM is generally performed to observe cross-sections of samples. To prepare the cross-section sample, the Ni-rich material foil is milled by the Ar-ion beam. Cross-sectional SEM of monodisperse particles can be observed by the obtained ion beam cross-section. Additionally, TEM, high-angle annular dark-field STEM, and fast Fourier transform were usually coupled to apply to SC materials to represent the structure evolution in detail [insert of Fig. 5(b)] [68]. 3D reconstruction as a type of calculation and modeling method has been introduced into the study of SC materials, which can show the stereoscopic morphology of an electrode during cycling [69]. Figure 5(c) shows the 3D reconstruction microstructure and SEM images of SC $LiNi_{0.6}Mn_{0.2}Co_{0.2}O_2$ after 100th and 200th cycles, in which the cracks can be clearly and accurately modeled in the sample after cycle. The 3D reconstruction microstructure combined with the 2D projection images extracted along the z vertical axis can obtain more information about the growth of the crack in the bulk material. By comparison with the corresponding SEM images, the crack evolution and electrochemical behavior in the 3D situation can be clarified during cycling. In addition, *in situ* XRD was performed to detect the structure change of SC Ni-rich materials during the charge-discharge process.

Fan *et al.* [70] clarified the structure change of the SC $LiNi_{0.88}Co_{0.09}Mn_{0.03}O_2$ cathode material during the initial charge-discharge process, in which the evolution of the layered phase structure is associated to Li contents [Fig. 5(d)]. More specially, *in situ* XRD can track phase transitions including H/M, M/H2, and H2/H3 within layered Ni-rich cathode materials during charge and discharge processes, which corresponds to the split and shift of the (003) diffraction peak. By means of *in situ* XRD measurement, not only can phase transitions be clearly observed but also lattice parameters and volume changes can be well elucidated, which is beneficial for clarifying the structural evolution of layered Ni-rich cathode materials upon cycling [32]. Based on these techniques, the morphology changes and structure evolutions of SC cathodes can be well illuminated, further shedding light on the development of high-energy-density and long-life next-generation cathode materials.

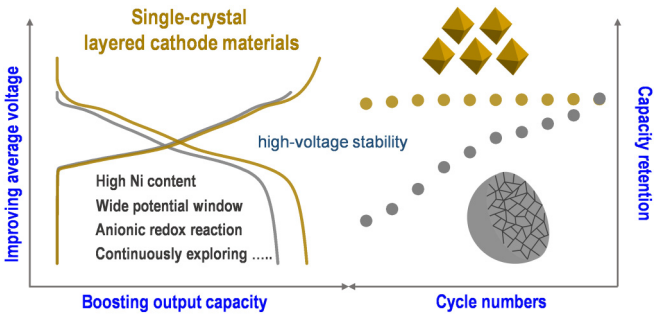

FIG. 6. Illustration of future development and prospect for single-crystal (SC) layered Ni-rich cathode materials.

VI. CONCLUSIONS AND PROSPECTIVE

In summary, the various strategies of high-temperature, multicalcination, spray pyrolysis, and the molten salt assistant method as well as the corresponding pros and cons are summarized for preparing SC Ni-rich layered cathode materials, which further provide a basic understanding of SC nickel-rich materials from the aspects of crystallography and materials physics. Furthermore, the comparisons of electrochemical behaviors and cycling performances between PC and SC electrodes were provided in both low- and high-voltage windows. Moreover, the morphology changes and phase transitions were presented within PC and SC electrodes upon cycling, which further clarifies the mechanisms of structural and electrochemical failures in SC and PC Ni-rich cathode materials. Additionally, state-of-the-art technologies were introduced to characterize the structural evolution of SC Ni-rich materials, further shedding light on the investigation of failure mechanisms in SC Ni-rich and other advanced cathode materials. In this review, we not only provided the fundamental understandings of SC layered Ni-rich oxides but also proposed a guideline for developing high-energy-density and long cycle life cathode materials for LIBs.

To harvest the advanced next-generation cathode materials based on SC morphology, improvements can be achieved along the avenue of modification and design strategies for PC cathodes. From the aspect of modification strategy, SC cathode materials possess the inherent advantages of low specific surface area and smooth particle surface, which is beneficial for further optimizations such as surface coating and physical modifications in comparison with PC counterparts [71,72]. In contrast, it is hard to effectively eliminate the microcracks in PC cathodes with secondary particles of several micrometers in diameter by a nanothickness surface layer. Benefiting from the elimination of internal grain boundaries and intergranular fracture, SC electrodes harvest remarkable high-voltage stability during cycling, which can be employed in a wide potential window to obtain high output capacities triggered by the combination of traditional cationic and anionic redox activities (Fig. 6) [66,73,74]. The energy density of Ni-rich cathode materials can be further boosted by increasing the Ni fractions based on SC morphology. Meanwhile, the issues generated in PC electrodes of microcracks and induced inferior cycling stability can be expected to be well addressed within SC Ni-rich cathode materials. Combined with excellent structural stability and great optimization potentials, they offer

immense opportunities in achieving superior electrochemical stability and high output capacity within advanced SC cathode materials during long-term cycling, which greatly promotes the realization of next-generation LIBs with high energy density and long life. On the other hand, from an application point of view, compared with PC Ni-rich materials, the SC obviously requires higher cost due to high preparation temperature and additional flux in the synthesis process. On the other hand, benefiting from high capacity and excellent cycle performance, the SC exhibits higher cost performance than the PC from the development perspective. Additionally, compared with the PC, the SC Ni-rich material is still in rapid development, which is still hopeful for further improvement in cost control in future research. Furthermore, the SC Ni-rich cathode is widely considered to possess excellent thermal stability to suppress harmful phenomena such as thermal runaway, which is prone to practical application. Benefiting from the low specific surface area and excellent structural stability, the SC can still show safe and stable electrochemical performance even at high-voltage and temperature conditions, which offer it strong potential. Finally, accompanied by the vigorous development of SC cathode materials, it can be expected that corresponding advanced characterization techniques will be further developed, which in turn promote the progress of engineering technology.

ACKNOWLEDGMENTS

This review was partially supported by the National Natural Science Foundation of China (No. 21633003 and No. U1801251). J.S. and X.C. acknowledge the scholarship from the China Scholarship Council.

[1] J. B. Goodenough and K. S. Park, The Li-ion rechargeable battery: A perspective, J. Am. Chem. Soc. **135**, 1167 (2013).

[2] K. Wang, B. Xue, Y. Tan, J. Sun, Q. Li, S. Shi, and Li P, Recycling of micron-sized Si powder waste from diamond wire cutting and its application in Li-ion battery anodes, J. Clean. Prod. **239**, 117997 (2019).

[3] Y. Tang, Y. Zhang, X. Rui, D. Qi, Y. Luo, W. Leow, S. Chen, J. Guo, J. Wei, W. Li *et al.*, Conductive inks based on a lithium titanate nanotube gel for high rate lithium-ion batteries with customized configuration, Adv. Mater. **28**, 1567 (2016).

[4] B. Li, J. Zheng, H. Zhang, L. Jin, D. Yang, H. Lv, C. Shen, A. Shellikeri, Y. Zheng, R. Gong *et al.*, Electrode materials, electrolytes, and challenges in nonaqueous lithium-ion capacitors, Adv. Mater. **30**, 1705670 (2018).

[5] S. Xia, X. Wu, Z. Zhang, Y. Cui, and W. Liu, Practical challenges and future perspectives of all-solid-state lithium-metal batteries, Chem. **5**, 753 (2019).

[6] P. Yan, J. Zheng, J. Liu, B. Wang, and X. Cheng, Tailoring grain boundary structures and chemistry of Ni-rich layered cathodes for enhanced cycle stability of lithium-ion batteries, Nat. Energy **3**, 600 (2018).

[7] W. Liu, P. Oh, X. Liu, M. Lee, W. Cho, S. Chae, Y. Kim, and J. Cho, Nickel-rich layered lithium transitional-metal oxide for high-energy lithium-ion batteries, Angew. Chem. Int. Ed. **54**, 4440 (2015).

[8] A. Manthiram, B. Song, and W. Li, A perspective on nickel-rich layered oxide cathodes for lithium-ion batteries, Energy Stor. Mater. **6**, 125 (2017).

[9] C. S. Yoon, K. J. Park, U. H. Kim, K. H. Kang, H. H. Ryu, and Y. K. Sun, High-energy Ni-rich $Li[Ni_xCo_yMn_{1-x-y}]O_2$ cathodes via compositional partitioning for next–generation electric vehicles, Chem. Mater. **29**, 10436 (2017).

[10] K. J. Park, J. Y. Hwang, H. H. Ryu, F. Maglia, S. J. Kim, P. Lamp, C. S. Yoon, and Y. K. Sun, Degradation mechanism of Ni-enriched NCA cathode for lithium batteries: Are microcracks really critical? ACS Energy Lett. **4**, 1394 (2019).

[11] J. Li, H. Li, W. Stone, R. Weber, S. Hy, and J. Dahn, Synthesis of single crystal $LiNi_{0.5}Mn_{0.3}Co_{0.2}O_2$ for lithium ion batteries, J. Electrochem. Soc. **164**, A3529 (2017).

[12] W. Li, H. Asl, Q. Xie, and A. Manthiram, Collapse of $LiNi_{1-x-y}Co_xMn_yO_2$ lattice at deep charge irrespective of nickel content in lithium-ion batteries, J. Am. Chem. Soc. **141**, 5097 (2019).

[13] Q. Ran, H. Zhao, Q. Wang, X. Shu, Y. Hu, S. Hao, M. Wang, J. Liu, M. Zhang, and H. Li, Dual functions of gradient phosphate polyanion doping on improving the electrochemical performance of Ni-rich $LiNi_{0.6}Co_{0.2}Mn_{0.2}O_2$ cathode at high cut-off voltage and high temperature, Electrochim. Acta. **299**, 971 (2019).

[14] Y. Huang, Y. Huang, and X. Hu, Enhanced electrochemical performance of $LiNi_{0.8}Co_{0.15}Al_{0.05}O_2$ by nanoscale surface modification with Co_3O_4, Electrochim. Acta **231**, 294 (2017).

[15] Z. Chen, Y. Liu, Z. Lu, R. Hu, J. Cui, H. Xu, Y. Ouyang, Y. Zhang, and M. Zhu, Plasma-assisted coating of nanosized SnO_2 on $LiNi_{0.5}Mn_{0.3}Co_{0.2}O_2$ cathodes for enhanced cyclic stability of lithium-ion batteries, J. Alloys Compd. **803**, 71 (2019).

[16] W. Tang, Z. Chen, F. Xiong, F. Chen, C. Huang, Q. Gao, T. Wang, Z. Yang, and W. Zhang, An effective etching-induced coating strategy to shield $LiNi_{0.8}Co_{0.1}Mn_{0.1}O_2$ electrode materials by $LiAlO_2$, J. Power Sources **412**, 246 (2019).

[17] J. Chen, L. Zhu, D. Jia, X. Jiang, Y. Wu, Q. Hao, X. Xia, Y. Ouyang, L. Peng, and W. Tang, $LiNi_{0.8}Co_{0.15}Al_{0.05}O_2$ cathodes exhibiting improved capacity retention and thermal stability due to a lithium iron phosphate coating, Electrochim. Acta. **312**, 179 (2019).

[18] X. Zeng, T. Jian, Y. Lu, L. Yang, W. Ma, Y. Yang, J. Zhu, C. Huang, S. Dai, and X. Xi, Enhancing high-temperature and high-voltage performances of single-crystal $LiNi_{0.5}Mn_{0.3}Co_{0.2}O_2$ cathodes through a $LiBO_2$/$LiAlO_2$ dual-modification strategy, ACS Sustain. Chem. Eng. **8**, 6293 (2020).

[19] Y. Han, S. Heng, Y. Wang, Q. Qu, and H. Zheng, Anchoring interfacial nickel cations on single-crystal $LiNi_{0.8}Co_{0.1}Mn_{0.1}O_2$ cathode surface via controllable electron transfer, ACS Energy Lett. **5**, 2421 (2020).

[20] H. Li, J. Li, X. Ma, and J. Dahn, Synthesis of single crystal $LiNi_{0.6}Co_{0.2}Mn_{0.2}O_2$ with enhanced electrochemical performance for lithium ion batteries, J. Electrochem. Soc. **165**, A1038 (2018).

[21] Y. Liu, J. Harlow, and J. Dahn, Microstructural observations of "single crystal" positive electrode materials before and after long term cycling by cross-section scanning electron microscopy, J. Electrochem. Soc. **167**, 020512 (2020).

[22] J. Li, L. E. Downie, L. Ma, W. Qiu, and J. Dahn, Study of the failure mechanisms of $LiNi_{0.8}Mn_{0.1}Co_{0.1}O_2$ cathode material for lithium ion batteries, J. Electrochem. Soc. **162**, A1401 (2015).

[23] E. Logan, H. Hebecker, X. Ma, J. Quinn, Y. HyeJeong, S. Kumakura, J. Paulsen, and J. Dahn, A comparison of the performance of different morphologies of $LiNi_{0.8}Co_{0.1}Mn_{0.1}O_2$ using isothermal microcalorimetry, ultra-high precision coulometry, and long-term cycling, J. Electrochem. Soc. **167**, 060530 (2020).

[24] Y. Liu, X. Fan, X. Huang, D. Liu, A. Dou, M. Su, and D. Chu, Electrochemical performance of $Li_{1.2}Ni_{0.2}Mn_{0.6}O_2$ coated with a facilely synthesized $Li_{1.3}Al_{0.3}Ti_{1.7}(PO_4)_3$, J. Power Sources **403**, 27 (2018).

[25] J. Li, H. Li, W. Stone, S. Glazier, and J. Dahn, Development of electrolytes for single crystal NMC532/artificial graphite cells with long lifetime, J. Electrochem. Soc. **165**, A626 (2018).

[26] L. Ma, S. Young, L. Ellis, Q. Huang, X. Ma, M. Chatzidakis, H. Li, L. Thompson, A. Eldesoky, C. McFarlane *et al.*, Impact of a titanium-based surface coating applied to $Li[Ni_{0.5}Mn_{0.3}Co_{0.2}]O_2$ on lithium-ion cell performance, ACS Appl. Energy Mater. **1**, 7052 (2018).

[27] Z. Wu, C. Cao, X. Yan, X. Zang, Y. Zhao, X. Ma, R. Liu, L. Hu, Y. Jiang, and S. Sun, Effects of charge cut-off voltage on the performances of monocrystalline $LiNi_{0.5}Mn_{0.3}Co_{0.2}O_2$/graphite Li-ion cells, Electrochim. Acta **302**, 153 (2019).

[28] B. Huang, D. Liu, K. Qian, L. Zhang, K. Zhou, Y. Liu, F. Kang, and B. Li, A simple method for the complete performance recovery of degraded Ni-rich $LiNi_{0.70}Co_{0.15}Mn_{0.15}O_2$ cathode via surface reconstruction, ACS Appl. Mater. Interfaces **11**, 14076 (2019).

[29] Y. Wang, E. Wang, X. Zhang, and H. Yu, High-voltage "single-crystal" cathode materials for lithium-ion batteries, Energy Fuels **35**, 1918 (2021).

[30] H. Sun and A. Manthiram, Impact of microcrack generation and surface degradation on a nickel-rich layered $Li[Ni_{0.9}Co_{0.05}Mn_{0.05}]O_2$ cathode for lithium-ion batteries, Chem. Mater. **29**, 8486 (2017).

[31] X. Guo, L. Hao, Y. Yang, Y. Wang, Y. Lu, and H. Yu, High cathode utilization efficiency through interface engineering in all-solid-state lithium metal batteries, J. Mater. Chem. A **7**, 25915 (2019).

[32] B. You, Z. Wang, F. Shen, Y. Chang, W. Peng, X. Li, H. Guo, Q. Hu, C. Deng, S. Yang *et al.*, Research progress of single-crystal nickel-rich cathode materials for lithium ion batteries, Small Methods **5**, 2100234 (2021).

[33] E. Trevisanello, R. Ruess, G. Conforto, F. Richter, and J. Janek, Polycrystalline and single crystalline NCM cathode materials-quantifying particle cracking, active surface area, and lithium diffusion, Adv. Energy Mater. **11**, 2003400 (2021).

[34] Q. Guo, J. Huang, Z. Liang, H. Potapenko, M. Zhou, X. Tang, and S. Zhong, The use of a single-crystal nickel-rich layered NCM cathode for excellent cycle performance of lithium-ion batteries, New J. Chem. **45**, 3652 (2021).

[35] Y. Kim, Lithium nickel cobalt manganese oxide synthesized using alkali chloride flux: Morphology and performance as a cathode material for lithium ion batteries, ACS Appl. Mater. Interfaces **4**, 2329 (2012).

[36] J. Leng, J. Wang, W. Peng, Z. Tang, S. Xu, Y. Liu, and J. Wang, Highly-dispersed submicrometer single-crystal nickel-rich layered cathode: Spray synthesis and accelerated lithium-ion transport, Small **17**, 2006869 (2021).

[37] H. Yu, Y. Qian, M. Otani, D. Tang, S. Guo, Y. Zhu, and H. Zhou, Study of the lithium/nickel ions exchange in the layered $LiNi_{0.42}Mn_{0.42}Co_{0.16}O_2$ cathode material for lithium ion batteries: Experimental and first-principles calculations, Energy Environ. Sci. **7**, 1068 (2014).

[38] T. Park, J. Lim, and J. Son, Effect of calcination temperature of size controlled microstructure of $LiNi_{0.8}Co_{0.15}Al_{0.05}O_2$ cathode for rechargeable lithium battery, Bull. Korean Chem. Soc. **35**, 357 (2014).

[39] J. Langdon and A. Manthiram, A perspective on single-crystal layered oxide cathodes for lithium-ion batteries, Energy Stor. Mater. **37**, 143 (2021).

[40] J. Duan, C. Wu, Y. Cao, D. Huang, K. Du, Z. Peng, and G. Hu, Enhanced compacting density and cycling performance of Ni-riched electrode via building mono dispersed micron scaled morphology, J. Alloys Compd. **695**, 91 (2017).

[41] M. Yi, J. Li, X. Fan, M. Bai, Z. Zhang, B. Hong, Z. Zhang, G. Hu, H. Jiang, and Y. Lai, Single crystal Ni-rich layered cathodes enabling superior performance in all-solid-state batteries with PEO-based solid electrolytes, J. Mater. Chem. A **9**, 16787 (2021).

[42] W. Li, X. Zhang, J. Si, J. Yang, and X. Sun, TiO_2-coated $LiNi_{0.9}Co_{0.08}Al_{0.02}O_2$ cathode materials with enhanced cycle performance for Li-ion batteries, Rare Met. **40**, 1719 (2021).

[43] J. Kim, H. Ma, H. Cha, H. Lee, J. Sung, M. Seo, P. Oh, M. Park, and J. Cho, A highly stabilized nickel-rich cathode material by nanoscale epitaxy control for high-energy lithium-ion batteries, Energy Environ. Sci. **11**, 1449 (2018).

[44] P. Kalyani and N. Kalaiselvi, Various aspects of $LiNiO_2$ chemistry: A review, Sci. Tech. Adv. Mater. **6**, 689 (2005).

[45] H. Zhang, S. Yang, Y. Huang, and X. Hou, Synthesis of non-spherical $LiNi_{0.88}Co_{0.09}Al_{0.03}O_2$ cathode material for lithium-ion batteries, Energy Fuels **34**, 9002 (2020).

[46] X. Cao and H. Zhou, An indicator of designing layered sodium-ion oxide materials, Sci. Bull. **66**, 753 (2021).

[47] G. Qian, Z. Li, D. Meng, J. Liu, Y. He, Q. Rao, Y. Liu, Z. Ma, and L. Li, Temperature-swing synthesis of large-size single-crystal $LiNi_{0.6}Co_{0.2}Mn_{0.2}O_2$ cathode materials, J. Electrochem. Soc. **168**, 010534 (2021).

[48] G. Qian, Y. Zhang, L. Li, R. Zhang, J. Xu, Z. Cheng, S. Xie, H. Wang, Q. Rao, Y. He *et al.*, Single-crystal nickel-rich layered-oxide battery cathode materials: Synthesis, electrochemistry, and intra-granular fracture, Energy Stor. Mater. **27**, 140 (2020).

[49] H. Cha, J. Kim, H. Lee, N. Kim, J. Hwang, J. Sung, M. Yoon, K. Kim, and J. Cho, Boosting reaction homogeneity in high-energy lithium-ion battery cathode materials, Adv. Mater. **32**, 2003040 (2020).

[50] T. Kimijima, N. Zettsu, and K. Teshima, Growth manner of octahedral-shaped $Li(Ni_{1/3}Co_{1/3}Mn_{1/3})O_2$ single crystals in molten Na_2SO_4, Cryst. Growth Des. **16**, 2618 (2016).

[51] S. Oishi, K. Teshima, and H. Kondo, Flux growth of hexagonal bipyramidal ruby crystals, J. Am. Chem. Soc. **126**, 4768 (2004).

[52] Y. Liu, L. Tang, H. Wei, X. Zhang, Z. He, Y. Li, and J. Zheng, Enhancement on structural stability of Ni-rich cathode

materials by *in-situ* fabricating dual-modified layer for lithium-ion batteries, Nano Energy **65**, 10 (2019).

[53] J. Lim, H. Kim, K. Cho, and M. Cho, Fundamental mechanisms of fracture and its suppression in Ni-rich layered cathodes: Mechanics-based multiscale approaches, Extreme Mech. Lett. **22**, 98 (2018).

[54] P. Pang, X. Tan, Z. Wang, Z. Cai, J. Nan, Z. Xing, and H. Li, Crack-free single-crystal $LiNi_{0.83}Co_{0.10}Mn_{0.07}O_2$ as cycling/thermal stable cathode materials for high voltage lithium-ion batteries, Electrochim. Acta **365**, 137380 (2021).

[55] S. Klein, P. Bärmann, O. Fromm, K. Borzutzki, J. Reiter, Q. Fan, M. Winter, T. Placke, and J. Kasnatscheew, Prospects and limitation of single-crystal cathode materials to overcome crosstalk phenomena in high-voltage lithium ion cells, J. Mater. Chem. A **9**, 7546 (2021).

[56] F. Wang, M. Ge, S. Wi, X. Liu, J. Bai, S. Ehrlich, D. Lu, W. Lee, and Z. Chen, Kinetic limitations in single-crystal high-nickel cathodes, Angew. Chem. Int. Ed. **60**, 17350 (2021).

[57] C. Zhan, J. Lu, A. Jeremy Kropf, T. Wu, A. Jansen, Y. Sun, X. Qiu, and K. Amine, Mn (II) deposition on anodes and its effects on capacity fade in spinel lithium manganate–carbon systems, Nat. Commun. **4**, 2437 (2013).

[58] J. Guo and W. Li, Synthesis of single-crystal $LiNi_{0.7}Co_{0.15}Mn_{0.15}O_2$ materials for Li-ion batteries by a Sol-Gel method, ACS Appl. Energy Mater. **5**, 397 (2021).

[59] C. Yang, R. Shao, Y. Mi, L. Shen, B. Zhao, K. Wu, W. Lui, P. Gao, and H. Zhou, Stable interstitial layer to alleviate fatigue fracture of high nickel cathode for lithium-ion batteries, J. Power Sour. **376**, 200 (2018).

[60] N. Yabuuchi, K. Yoshii, S.-T. Myung, I. Nakai, and S. Komaba, Detailed studies of a high-capacity electrode material for rechargeable batteries, Li_2MnO_3-$LiCo_{1/3}Ni_{1/3}Mn_{1/3}O_2$, J. Am. Chem. Soc. **133**, 4404 (2011).

[61] X. Fan, G. Hu, B. Zhang, X. Ou, J. Zhang, W. Zhao, H. Jia, L. Zou, P. Li, and Y. Yang, Crack-free single-crystalline Ni-rich layered NCM cathode enable superior cycling performance of lithium-ion batteries, Nano Energy **70**, 104450 (2020).

[62] W. Li, X. Liu, H. Celio, P. Smith, A. Dolocan, M. Chi, and A. Manthiram, Mn versus Al in layered oxide cathodes in lithium-ion batteries: A comprehensive evaluation on long-term cyclability, Adv. Energy Mater. **8**, 1703154 (2018).

[63] K. Min, C. Jung, D. S. Ko, K. Kim, J. Jang, K. Park, and E. Cho, High-performance and industrially feasible Ni-rich layered cathode materials by integrating coherent interphase, ACS Appl. Mater. Interfaces **10**, 20599 (2018).

[64] Y. Su, Q. Zhang, L. Chen, L. Bao, Y. Lu, S. Chen, and F. Wu, Stress accumulation in Ni-rich layered oxide cathodes: Origin, impact, and resolution, J. Energy Chem. **65**, 236 (2022).

[65] U. H. Kim, H. H. Ryu, J. H. Kim, R. Mücke, P. Kaghazchi, C. S. Yoon, and Y. K. Sun, Microstructure-controlled Ni-rich cathode material by microscale compositional partition for next-generation electric vehicles, Adv. Energy Mater. **9**, 1803902 (2019).

[66] J. Sun, C. Sheng, X. Cao, P. Wang, P. He, H. Yang, Z. Chang, X. Yue, and H. Zhou, Restraining oxygen release and suppressing structure distortion in single-crystal Li-rich layered cathode materials, Adv. Funct. Mater. **32**, 2110295 (2021).

[67] Y. Bi, J. Tao, Y. Wu, L. Li, Y. Xu, E. Hu, B. Wu, J. Hu, C. Wang, J. Zhan *et al.*, Reversible planar gliding and microcracking in a single-crystalline Ni-rich cathode, Science **370**, 1313 (2020).

[68] W. Wei, Z. Ding, C. Chen, C. Yang, B. Han, L. Xiao, C. Liang, P. Gao, and K. Cho, Surface-dependent stress-corrosion cracking in Ni-rich layered oxide cathodes, Acta Materialia. **212**, 116914 (2021).

[69] F. Zhang, S. Lou, S. Li, Z. Yu, Q. Liu, A. Dai, C. Cao, M. Toney, M. Ge, X. Xiao *et al.*, Surface regulation enables high stability of single-crystal lithium-ion cathodes at high voltage, Nat. Commun. **11**, 3050 (2020).

[70] X. Fan, X. Ou, W. Zhao, Y. Liu, B. Zhang, J. Zhang, L. Zou, L. Seidl, Y. Li, G. Hu *et al.*, *In situ* inorganic conductive network formation in high-voltage single-crystal Ni-rich cathodes, Nat. Commun. **12**, 5320 (2021).

[71] W. Liu, X. Sun, X. Zhang, C. Li, K. Wang, W. Wen, and Y. Ma, Structural evolution of mesoporous graphene/$LiNi_{1/3}Co_{1/3}Mn_{1/3}O_2$ composite cathode for Li-ion battery, Rare Met. **40**, 521 (2021).

[72] X. Cao, H. Li, Y. Qiao, M. Jia, P. He, J. Cabana, and H. Zhou, Achieving stable anionic redox chemistry in Li-excess O2-type layered oxide cathode via chemical ion-exchange strategy, Energy Stor. Mater. **38**, 1 (2021).

[73] X. Cao, H. Li, Y. Qiao, M. Jia, H. Kitaura, J. Zhang, P. He, J. Cabana, and H. Zhou, Structure design enables stable anionic and cationic redox chemistry in a T2-type Li-excess layered oxide cathode, Sci. Bull. **67**, 381 (2021).

[74] X. Cao, Qiao, M. Jia, P. He, and H. Zhou, Ion-exchange: A promising strategy to design Li-rich and Li-excess layered cathode materials for Li-ion batteries, Adv. Energy Mater. **12**, 2003972 (2021).